Chinese Journal of Polymer Science Vol. 35, No. 5, (2017), 623–630

Chinese Journal of Polymer Science
© Chinese Chemical Society
Institute of Chemistry, CAS
Springer-Verlag Berlin Heidelberg 2017

Patterning of Triblock Copolymer Film and Its Application for Surface-enhanced Raman Scattering*

Hai-liang Huang, Guo-bin Yi**, Xi-hong Zu, Ben-bin Zhong and Hong-sheng Luo
School of Chemical Engineering and Light Industry, Guangdong University of Technology, Guangzhou 510006, China

Abstract In this paper, microphase behavior of an ABC triblock copolymer, polystyrene-block-poly(2-vinylpyridine)-block-poly(ethylene oxide), namely PS-*b*-P2VP-*b*-PEO, was systematically studied during spin-coating and solvent vapor annealing based on various parameters, including the types of the solvent, spin speed and thickness. The morphological features and the microdomain location of the different blocks were characterized by atomic force microscope (AFM) and high resolution transmission electron microscopy (HRTEM). With increasing thickness, the order-order transition from nanopores array to the pattern of nanostripes was observed due to microdomain coarsening. These processes of pattern transformation were based on the selectivity of toluene for different blocks and on the contact time between solvent molecules and the three blocks. This work provides different templates for preparation of gold nanoparticle array on silicon wafer, which can be adopted as an active surface-enhanced Raman scattering (SERS) substrate for poly(3-hexylthiophene) (P3HT).

Keywords Self-assembly; Triblock copolymer; Nanopattern; Nanoparticle array; Raman spectroscopy

INTRODUCTION

Amphiphilic triblock copolymers attract increasing attention in the area of self-assembly, since their self-assembly generates highly ordered periodic nanostructures[1–4], which have various applications[5–11], including deposition of inorganic particles, drug delivery, bioengineering, membranes, nanolithography, organic photovoltaics, to name a few.

As an effective nanostructured template to synthesize and organize nanoparticles in a controlled manner, self-assembled nanodomains of triblock copolymers have been employed[12]. In recent years, Raman spectroscopy has been developed from conventional laboratory system to portable handheld device for rapid on-site detection with the emerging applications of surface-enhanced Raman scattering (SERS), including environmental monitoring[13–15], biochemistry[16, 17] and chemical production[18, 19]. Recently, Duan *et al.* reported the development of bioconjugated plasmonic vesicles assembled from SERS-encoded amphiphilic gold nanoparticles for cancer-targeted drug delivery, which can play multifunctional roles as delivery carriers for anticancer drugs and SERS-active plasmonic imaging probes to specifically label targeted cancer cells and monitor intracellular drug delivery[20]. With all the advantages offered by SERS, many studies have been directed toward fabricating an ideal SERS substrate, such as particle-in-bowl arrays[21], nanowire/nanoparticle composite arrays[22, 23], nanowire arrays[24], monodispersed nanoparticles[25] and nanodimple array[26].

Although polystyrene-block-poly(2-vinylpyridine)-block-poly(ethylene oxide), *i.e.* PS-*b*-P2VP-*b*-PEO, has

* This work was financially supported by the National Natural Science Foundation of China (Nos. 51273048 and 51203025) and Natural Science Foundation of Guangdong Province (No. S2012040007725).
** Corresponding author: Guo-bin Yi (易国斌), E-mail: ygb702@163.com
Received September 20, 2016; Revised October 18, 2016; Accepted October 18, 2016
doi: 10.1007/s10118-017-1914-9

been extensively studied, including the crystallization process of PEO block[27–30] and hydrophilicity difference between diblock copolymers polystyrene-block-poly(2-vinylpyridine) (PS-*b*-P2VP) and PS-*b*-P2VP-*b*-PEO[31], systematic study on the nanopattern transformation of PS-*b*-P2VP-*b*-PEO thin films during spin-coating is limited. A systematic study is important for large-area and economical preparation of ordered gold nanoparticle array which could be used as an active SERS substrate[32].

In this work, we focus on a systematic study on the effect of different process conditions during spin-coating on the different nanoscale structures of PS-*b*-P2VP-*b*-PEO thin films. Furthermore, the microdomain location of the three blocks in PS-*b*-P2VP-*b*-PEO during spin-coating is also discussed in detail. Additionally, patterned PS-*b*-P2VP-*b*-PEO thin films are used as template to fabricate large-area and well-ordered Au nanoparticle arrays on silicon substrates for enhancing Raman intensity of poly(3-hexylthiophene) (P3HT) by SERS. This work will promote the use of ordered nanopattern of ultrathin triblock copolymer films in a wide area.

EXPERIMENTAL

Materials

Triblock copolymers, polystyrene-block-poly(2-vinylpyridine)-block-poly(ethylene oxide) (PS-*b*-P2VP-*b*-PEO with molecular weight of 45000, 16000 and 8500 and molecular weight polydispersity of M_w/M_n = 1.05), were purchased from Polymer Source Inc. and used without further purification. $HAuCl_4 \cdot 3H_2O$ (99%, Au ≥ 49%) was purchased from Alfa Aesar of Thermo Fisher Scientific Ltd. P3HT (M_w = 30000) was purchased from J&K Scientific Co., Ltd., China. Chloroform ($CHCl_3$) was purchased from Guangzhou Chemical Reagent Factory. Toluene (99+%), tetrahydrofuran (THF) and *N*,*N*′-dimethylformamide (DMF, analytical grade) were purchased from Tianjin Damao Chemical Co., Ltd. Silicon (Si) wafer <100> was purchased from No. 46 Research Institute of China Electronics Technology Group Corporation (CETC).

Preparation of Triblock Copolymer Thin Film

Si wafer was utilized as substrate to prepare PS-*b*-P2VP-*b*-PEO films. Si wafers were cleaned in DMF, ethanol and deionized water with ultrasonic cleaner for 30 min at room temperature, subsequently. The triblock polymer PS-*b*-P2VP-*b*-PEO was dissolved in toluene (at concentration of 0.1 wt%, 0.2 wt%, 0.4 wt%, 0.6 wt% and 1 wt%) and stirred for 24 h at room temperature. Thin films of PS-*b*-P2VP-*b*-PEO were prepared by spin-coating at different spin speed (2000, 3000 and 4000 r/min) on silicon substrate (relative humidity: 65%–95%).

Preparation of Gold Nanoparticle Array

The films spin-coated from PS-*b*-P2VP-*b*-PEO toluene solution (0.1 wt%) were immersed in an ethanol solution of hydrogen tetrachloroauratetrihydrate ($HAuCl_4 \cdot 3H_2O$, 0.41 wt%) for 90 min. The films were then rinsed with ethanol several times to remove any free Au-salt and thoroughly dried in air. The thin films of PS-*b*-P2VP-*b*-PEO containing Au salts were then exposed to air plasma for 20 min and calcinated for 9 h at 600 °C to remove the PS-*b*-P2VP-*b*-PEO thin films.

Preparation of P3HT Films

P3HT films on Au nanoparticle arrays were prepared by spin-coating from a solution of P3HT (5 mg/mL in chlorobenzene) on the substrates at 3000 r/min with a fixed volume (30 μL). All samples were dried in a vacuum oven for at least 12 h to remove the residual solvent. The samples were kept in a dark space to prevent deterioration.

Characterization

Atomic force microscope (AFM) in SCANASYST-AIR mode (Nanoscope-V Multimode 8, Bruker Inc., Germany) by using a silicon cantilever (spring constant 5 N/m and resonant frequency ~150 kHz, Budget Sensors, Bulgaria Ltd.) was used to investigate the morphological features of PS-*b*-P2VP-*b*-PEO thin films. The thickness of film was measured by a spectroscopic ellipsometry over a wavelength range of 400–1700 nm using a V-VASE spectroscopic ellipsometer (J.A. Woollam, USA). High resolution transmission electron microscopy

(HRTEM) measurements was carried out on a JEM-2100HR (JEOL, Japan) operated at 200 kV accelerating voltage. Film samples for TEM were prepared onto carbon-coated copper grids. Some of the samples were exposed to I_2 vapor for certain period. Field-emission scanning electron microscopy (FE-SEM, JEOL JSM-7001F, Japan) was operated at 15 kV. Image J software was utilized to analyze the nanoparticle size and size distribution. Raman spectroscopic analysis was performed on a Lab RAM HR800 micro-Raman spectrometer equipped with an Ar ion laser as the excitation resource (633 nm).

RESULTS AND DISCUSSION

The effect of the solvent for polymer solution is shown in Fig. 1. These films were spin-coated from 0.1 wt% PS-*b*-P2VP-*b*-PEO solution (0.1 wt%) on the silicon wafers with 3000 r/min at room temperature. Toluene, chloroform and tetrahydrofuran (THF) were used as solvents, respectively. Microphase-separated pattern of holes could be obviously seen when toluene was used as the solvent (Fig. 1b). On the other hand, the nanopattern of the films spin-coated from chloroform (boiling point of 62 °C) and THF (boiling point of 66 °C) were disordered as shown in Figs. 1(a) and 1(c). Thus, the control of spin-coating process was weakened with increasing solvent volatility[33]. In addition, the difference of the selective solubility of toluene with regard to the three blocks in PS-*b*-P2VP-*b*-PEO was larger than $CHCl_3$ and THF. Toluene was a good solvent for PS block, but poor for P2VP and PEO blocks, which was beneficial to microphase separation of PS-*b*-P2VP-*b*-PEO during the process of spin-coating. Based on the volatility and solubility selectivity of the solvents, toluene was the optimal solvent for PS-*b*-P2VP-*b*-PEO copolymer solution and the self-assembly during spin-coating with low solvent volatility (The boiling point of toluene was 110.6 °C).

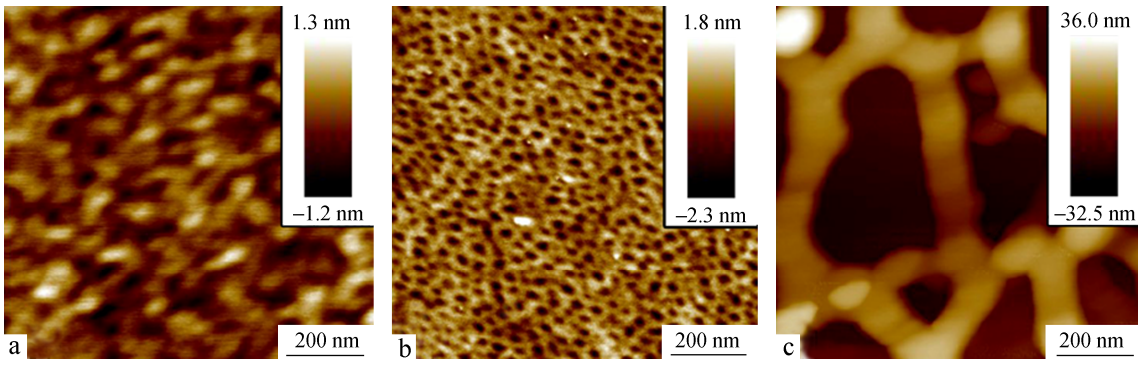


Fig. 1 AFM height images of PS-*b*-P2VP-*b*-PEO films spin-coated from 0.1 wt% PS-*b*-P2VP-*b*-PEO solution with three different solvents at 3000 r/min on silicon substrate: (a) chloroform, (b) toluene and (c) tetrahydrofuran

The influence of spin speed is shown in Fig. 2. The films with three different nanopatterns were spin-coated from PS-*b*-P2VP-*b*-PEO toluene solution (0.1 wt%) with various spin speeds. When the spin speed was 2000 r/min, the low evaporation rate and small centrifugal force led to the inhomogeneous distribution of PS-*b*-P2VP-*b*-PEO, resulting in a pattern with a few irregular holes observed in rough surface (Fig. 2a). When the spin speed was 3000 r/min, appropriate evaporation rate would lead to an adequate movement of the molecular chains, resulting in the formation of ordered nanoporous pattern (Fig. 1b). When the spin speed increased to 4000 r/min, the molecular chains would be frozen before their adequate movement because of too fast evaporation rate, resulting in disordered nanoporous pattern with various sizes (Fig. 2b). The solvent evaporation rate during spin-coating was proportional to the spin speed, which controlled phase separation and domain coarsening[34]. Changes in spin speed provided a method to systematical change for the solvent evaporation rate. These results demonstrated that both 2000 and 4000 r/min caused disordered arrangement of the molecular chains when the thickness was 8.560 nm, and the spin speed should be controlled at 3000 r/min in the process of spin-coating to obtain an ordered nanopattern of PS-*b*-P2VP-*b*-PEO.

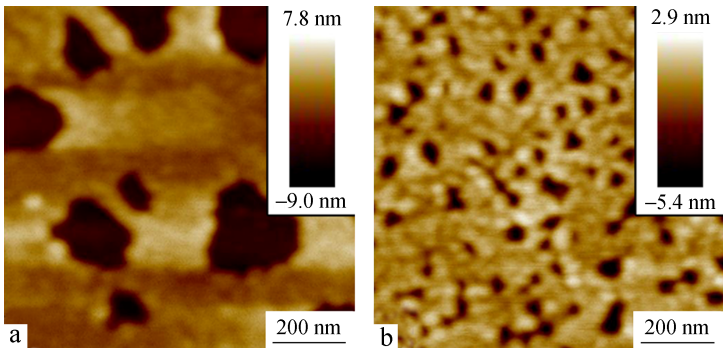


Fig. 2 AFM height images of PS-*b*-P2VP-*b*-PEO films spin-coated on silicon wafers from its toluene solution (0.1 wt%) at different spin speeds: (a) 2000 r/min and (b) 4000 r/min

The films of PS-*b*-P2VP-*b*-PEO of different thickness spin-coated with different concentrations are presented in Fig. 3. When the thickness was 8.560 nm (0.1 wt%), nanoporous pattern was given in Fig. 1(b) with the average diameter of holes about 26 nm. When the thickness was 22.594 nm (0.2 wt%), a large part of pores held their position, but a strong tendency to transit into the structure of stripe was shown in Fig. 3(a). In Fig. 3(b), the pattern of the stripe became the majority with the decreasing number of the pores when the thickness was 29.959 nm (0.4 wt%). The average diameter of the holes was about 26 nm, and the average width of the stripe was about 25 nm. With an increase in the thickness to 52.690 nm (0.6 wt%, Fig. 3c), the average width of the stripe was about 30 nm, which was larger than the former (0.4 wt%). The average diameter of holes was about 28 nm. The spacing between the nanostripes was also more compact than the former. When the thickness increased to 87.276 nm (1 wt%), a pattern of the stripe with less pores appeared as shown in Fig. 3(d). The average width of the stripes was about 34 nm and the average diameter of the pores was about 30 nm.

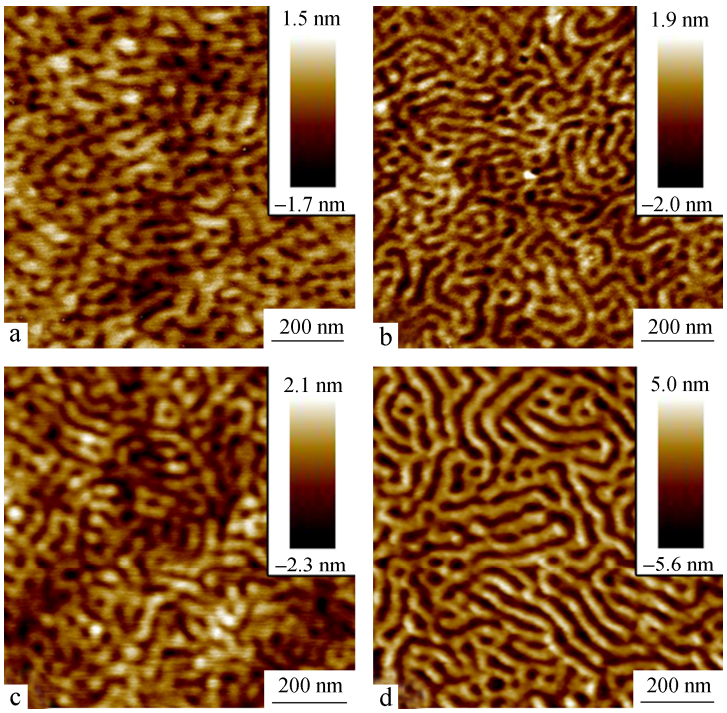


Fig. 3 AFM height images of the PS-*b*-P2VP-*b*-PEO films with various thickness: (a) 22.594 nm, (b) 29.959 nm, (c) 52.690 nm and (d) 87.276 nm

As we all know, the triblock copolymer solution spreads uniformly on the substrate to form a liquid film during spin-coating, which is controlled by competition between centrifugal and viscous forces[34, 35]. The viscous forces increase with increasing solution concentration, restricting film thinning. And a thicker film provides a longer period of time for the solvent to evaporate and for microphase separation and domain coarsening. Considering the component of PS-*b*-P2VP-*b*-PEO and the selectivity of toluene for three blocks, the process of nanopattern transformation from nanopores to nanostripes will occur with increasing thickness, which indicates that the continuous matrix in different thickness should consist of PS block, and the microdomains of P2VP and PEO should be the dispersed phases.

In order to further clarify the microdomain location of the three blocks in thickness (8.560, 29.959 and 87.276 nm), various films were further investigated by TEM with or without staining the P2VP block by I_2. Because the effect of tip amplification for AFM was inevitable, the size of the nanopores and the nanostripes in AFM height images was larger than that of those structures (corresponding images) in TEM images after selective staining.

When the thickness was 8.560 nm (0.1 wt%), the image without staining was shown in Fig. 4(a). The holes appeared as bright regions (which matched with Fig. 1a) because of the thickness difference. However, dark rings around the holes were observed after the selective staining of the P2VP block, implying that the periphery of the holes corresponded to the P2VP block (Fig. 4b). Thus, the rest of the holes should match with the PEO block. The continuous matrix was the PS block. Each hole consisted of the P2VP and PEO blocks. Considering the sequence of the three blocks in PS-*b*-P2VP-*b*-PEO copolymers, the hole has to be a hollow cylindrical nanostructure. The average outer diameter of holes was about 23 nm. These holes could result from the cavity formation of the P2VP and PEO blocks by spin-coating in a high-humidity (65%–95%). Because both P2VP and PEO blocks could be swollen by water, kinetically frozen holes were formed by evaporation of water after vitrification of the PS block by fast evaporation of the solvent during the spin coating. A similar cavitation was reported for poly(acrylic acid) (PAA) domains in PS-*b*-PAA diblock copolymer because of the swelling of PAA by water[36].

With the thickness increased to 29.959 nm (0.4 wt%), the image without staining is shown in Fig. 4(c). The stripes occupied the dominance with a few of dots. Then the films displayed a sphere-in-depressed stripe structure after the selective staining for P2VP block. And dark rings, corresponding to P2VP block, were seen at the edge of those spheres (Fig. 4d). Thus the rest part of those spheres should be consisting of the PEO block. Hence, the continuous matrix was PS block. The outer average diameter of the dark rings was still around 18 nm. The average width of the nanostripes was about 25 nm. Because a thicker film, spin-coated from higher concentration, provided a longer period of time for the solvent to evaporate, toluene molecules had more time to be in contact with the three blocks. Moreover, toluene was a good solvent for PS but poor for the other blocks of P2VP and PEO, which promoted the structural transformation from pores to stripes. Thus, a lot of pores, corresponding to P2VP and PEO microdomains were wrapped by the PS block to decrease the interface between toluene molecules and the hydrophilic segments of PS-*b*-P2VP-*b*-PEO, resulting in decreasing number of nanopores, as shown in Fig. 3(b).

For the thickest film (87.276 nm, 1 wt%), the pattern of fuzzy stripes appeared as shown in Fig. 4(e). However, a few black dots and dark rings were also observed at the end of stripes after P2VP block staining, implying that the dots and the rings corresponded to the P2VP block (Fig. 4f). The bright region in those rings consisted of PEO block and the rest of the stripes consisted of the PS blocks. The average width of the stripe was about 28 nm, which was wider than that of the stripe shown in Fig. 4(f). The average outer diameter of the dark rings was about 23 nm. Because the contact time of the solvent molecules with the three blocks would be further prolonged with additionally increased concentration from 0.4 wt% to 1 wt%, the nanostripes coarsening would occur with the aggregation of the P2VP and PEO blocks, resulting in a further decreased number of the nanopores.

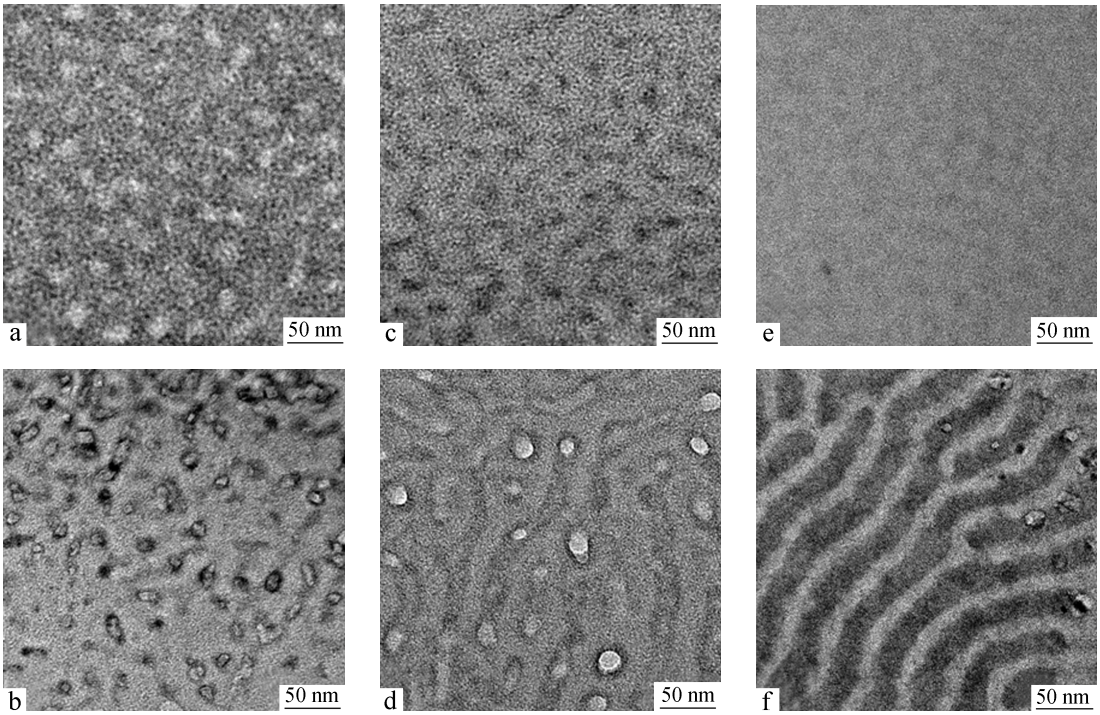


Fig. 4 TEM images of PS-*b*-P2VP-*b*-PEO film with different thickness: (a) 8.560 nm without I_2 staining, (b) 8.560 nm after I_2 staining, (c) 29.959 nm without I_2 staining, (d) 29.959 nm after I_2 staining, (e) 87.276 nm without I_2 staining and (f) 87.276 nm after I_2 staining

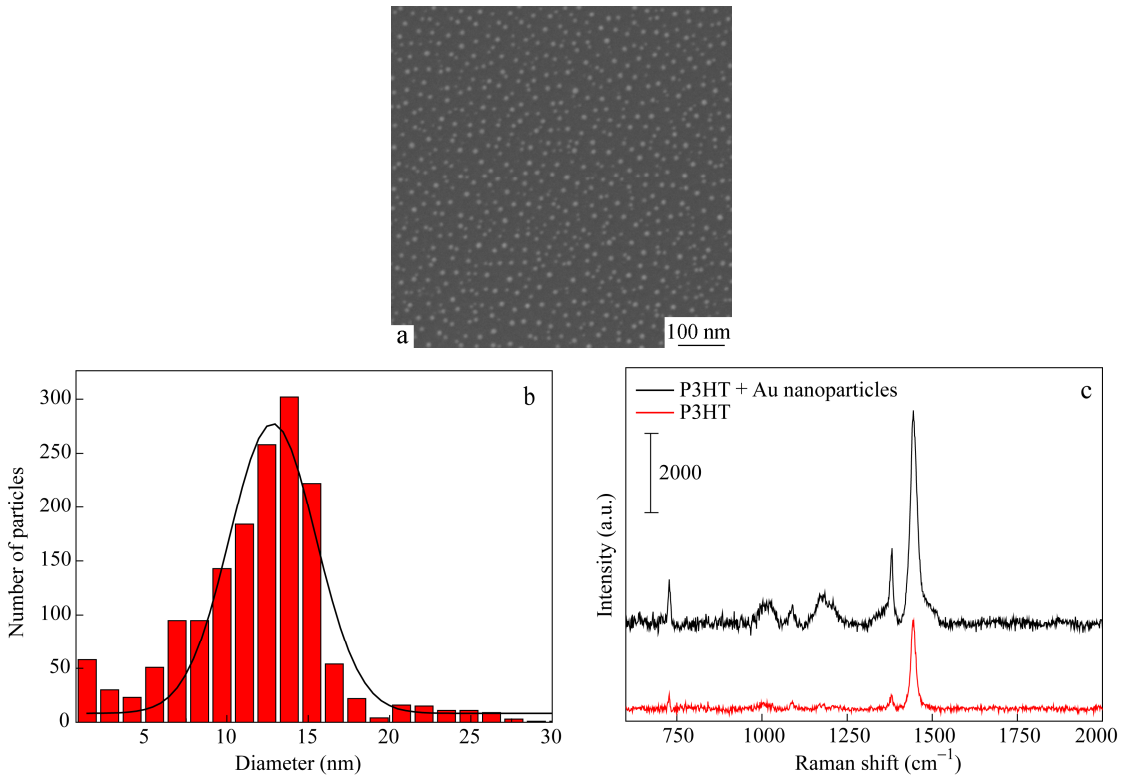


Fig. 5 (a) SEM image of gold nanoparticle array; (b) Diameter distribution diagrams of gold nanoparticle array; (c) Raman spectra of the P3HT films on bare silicon substrate and Au nanoparticle array

The nanopattern shown in Fig. 1(b), spin-coated from PS-*b*-P2VP-*b*-PEO toluene solution (0.1 wt%) was used as template to prepare gold nanoparticle array, as shown in Fig. 5(a). The average size of the gold nanoparticles was 13 nm (Fig. 5b) and the average interparticle distance was 25.94 nm. In order to demonstrate SERS performance of the ordered Au nanoparticle array on silicon substrate, P3HT was used as the target molecule. Compared with Raman signals of P3HT film on bare silicon substrate, the characteristic peaks intensity of P3HT films on the Au nanoparticle array was enhanced due to electromagnetic field enhancement based on the localized surface plasmon resonances (LSPR) of the gold nanoparticle and the electromagnetic coupling among the gold nanoparticles (Fig. 5c)[14].

CONCLUSIONS

We have systematically studied various parameters of the microphase separation for PS-*b*-P2VP-*b*-PEO, including the effect of solvent, spin speed and thickness of the film. The process of morphology evolution from the nanoporous array to a pattern of stripe was observed *via* increasing thickness of the film. Many nanostructures could be obtained due to the contact period among the solvent molecules and the three blocks in different thickness. On the other hand, the selectivity of toluene towards PS block and P2VP block also played an important role in the process of structural transformation. The patterned PS-*b*-P2VP-*b*-PEO thin films could be used as the template to prepare gold nanoparticle array, which could be used as an effective surface-enhanced Raman scattering substrate. Because of electromagnetic enhancement based on the localized surface plasmon resonances, Raman intensity of P3HT on Au nanoparticle array was much stronger than that on the bare silicon substrate. This work provides a simple approach to precisely control microdomains location in the triblock copolymers for preparation of gold nanoparticle array, which can be further used as an active surface-enhanced Raman scattering substrate. It has great potential applications as the sensors for biomolecules and in nanolithography, pattern transfer, bioengineering, membranes and other areas of interests.

REFERENCES

1 Xu, J.P., Wang, K., Li, J.Y., Zhou, H.M., Xie, X.L. and Zhu, J.T., Macromolecules, 2015, 48(8): 2628
2 Xu, J.P., Yang, Y., Wang, K., Li, J.Y., Zhou, H.M., Xie, X.L. and Zhu, J.T., Langmuir, 2015, 31(40): 10975
3 Tang, C.B., Lennon, E.M., Fredrickson, G.H., Kramer, E.J. and Hawker, C.J., Science, 2008, 322(5900): 429
4 Cui, H.G., Chen, Z.Y., Zhong, S., Wooley, K.L. and Pochan, D.J., Science, 2007, 317(5838): 647
5 Higuchi, T., Sugimori, H., Yabu, H. and Jinnai, H., Polym. J., 2016, 48(4): 509
6 Gu, X.D., Dorsey, P. and Russell, T.P., Adv. Mater., 2012, 24(40): 5505
7 Li, L., Lu, B.B., Fan, Q.K., Wei, L.L., Wu, J.N., Hou, J., Guo, X.H. and Liu, Z.Y., RSC Adv., 2016, 6(32): 27102
8 Im, S.H., Jeong, U. and Xia, Y.N., Nat. Mater., 2005, 4(9): 671
9 Ge, X.M., Duan, S.Y., Wu, F., Feng, J., Zhu, H. and Jin, T., Adv. Funct. Mater., 2015, 25(27): 4352
10 Ludwigs, S., Böker, A., Voronov, A., Rehse, N., Magerle, R. and Krausch, G., Nat. Mater., 2003, 2(11): 744
11 Fujita, H., Michinobu, T., Fukuta, S., Koganezawa, T. and Higashihara, T., ACS Appl. Mater. Interfaces, 2016, 8(8): 5484
12 Jeon, S.M., Jang, K.Y., Lee, S.H., Park, H.W. and Sohn, B.H., Langmuir, 2008, 24(19): 11137
13 Li, J.F., Huang, Y.F., Ding, Y., Yang, Z.L., Li, S.B., Zhou, X.S., Fan, F.R., Zhang, W., Zhou, Z.Y., Wu, D.Y., Ren, B., Wang, Z.L. and Tian, Z.Q., Nature, 2010, 464(7287): 392
14 Zu, X.H., Jian, Z.H., Yi, G.B., Huang, H.L., Zhong, B.B., Luo, H.S., Huang, J.R. and Wang, C., Chinese J. Polym. Sci., 2015, 33(10): 1470
15 Yin, J., Wu, T., Song, J.B., Zhang, Q., Liu, S.Y., Xu, R. and Duan, H.W., Chem. Mater., 2011, 23(21): 4756
16 Long, K.L., Luo, X.G., Nan, H.Y., Du, D.Y., Zhao, W.W., Ni, Z.H. and Qiu, T., Appl. Phys. Lett., 2013, 114(18): 183520

17 Premasiri, W.R., Lee, J.C., Sauer-Budge, A., Théberge, R., Costello, C.E. and Ziegler, L.D., Anal. Bioanal. Chem., 2016, 408(17): 4631
18 Indrasekara, A.S.D.S., Meyers, S., Shubeita, S., Feldman, L.C., Gustafsson, T. and Fabris, L., Nanoscale, 2014, 6(15): 8891
19 Zhang, J.R., Qiu, T., Yuan, H.F. and Li, X.Y., Chinese J. Polym. Sci., 2013, 31(3): 434
20 Song, J.B., Zhou, J.J. and Duan, H.W., J. Am. Chem. Soc., 2012, 134(32): 13458
21 Li, X.L., Zhang, Y.Z., Shen, Z.X. and Fan, H.J., Small, 2012, 8(16): 2548
22 Chen, L.M., Jiang, D., Liu, X.H. and Qiu, G.Z., ChemPhysChem, 2014, 15(8): 1624
23 Zhang, C.X., Liu, L., Yin, H.J., Fang, H., Zhao, Y.M., Bi, C.J. and Xu, H.J., Appl. Phys. Lett., 2014, 105(1): 011905
24 Sun, X.C., Stagon, S., Huang, H.C., Chen, J. and Lei, Y., RSC Adv., 2014, 4(45): 23382
25 Dou, X., Chung, P.Y., Sha, H.Y., Lin, Y.C. and Jiang, P., Phys. Chem. Chem. Phys., 2013, 15(30): 12680
26 Cassar, R.N., Graham, D., Larmour, I., Wark, A.W. and Faulds, K., Vib. Spectrosc., 2014, 71: 41
27 Huang, W.H., Luo, C.X., Zhang, J.L. and Han, Y.C., J. Chem. Phys., 2007, 126(10): 104901
28 Huang, W.H., Luo, C.X., Zhang, J.L., Yu, K. and Han, Y.C., Macromolecules, 2007, 40(22): 8022
29 Huang, W.H., Luo, C.X., Li, B.Y. and Han, Y.C., Macromolecules, 2006, 39(23): 8075
30 Huang, W.H., Luo, C.X., Wang, H.F. and Han, Y.C., Polym. Int., 2010, 59(8): 1064
31 Jung, A., Filiz, V., Rangou, S., Buhr, K., Merten, P., Hahn, J., Clodt, J., Abetz, C. and Abetz, V., Macromol. Rapid Commun., 2013, 34(7): 610
32 Lee, D.H., Park, S., Gu, W.Y. and Russell, T.P., ACS Nano, 2011, 5(2): 1207
33 Sinturel, C., Vayer, M., Morris, M. and Hillmyer, M.A., Macromolecules, 2013, 46(14): 5399
34 Fang, L., Wei, M., Barry, C. and Mead, J., Macromolecules, 2010, 43(23): 9747
35 Knoll, A., Horvat, A., Lyakhova, K.S., Krausch, G., Sevink, G.J.A., Zvelindovsky, A.V. and Magerle, R., Phys. Rev. Lett., 2002, 89(3): 035501
36 Boontongkong, Y. and Cohen, R.E., Macromolecules, 2002, 35(9): 3647